Topological Stabilization via Higgs and Z-Boson Repulsions in Electroweak Monopole-Antimonopole Pairs

Dan Zhu[1], Xurong Chen[1], and Khai-Ming Wong[2]

[1]Southern Center for Nuclear Science Theory, Institute of Modern Physics,
Chinese Academy of Sciences, Huizhou, 516000, China
School of Nuclear Science and Technology, University of Chinese Academy of Sciences, Beijing, 100049, China
[2] School of Physics, Universiti Sains Malaysia, 11800 USM, Penang, Malaysia

Presented by Dr. Dan Zhu
Institute of Modern Physics, Chinese Academy of Sciences
IHEP, Beijing — September 13, 2026

Introduction

- **Initial goal:**
  General properties of the Cho-Maison monopole-antimonopole pairs (MAPs).

- **MAP solutions in the Weinberg-Salam model:**
  D. Zhu, K. M. Wong and G. Q. Wong, *Commun. Theor. Phys.* **76**, 035201 (2024)

- **Cho-Maison monopole — topological origin and stability:**
  Y. M. Cho and D. Maison, *Phys. Lett. B* **391**, 360 (1997);
  Y. Yang, *Proc. R. Soc. Lond. A* **454**, 155 (1998);
  J. B. Mcleod and C. B. Wang, *Proc. R. Soc. Lond. A* **457**, 773 (2001);
  R. Gervalle and M. S. Volkov, *Nucl. Phys. B* **984**, 115937 (2022); **987**, 116112 (2023).

- **Generality:**
  The balancing mechanism reported in this talk is **not** tied to the singular Cho-Maison monopole. The same Higgs and Z-boson repulsions also operate in finite-energy configurations carrying *no magnetic charge*, like the electroweak vortex rings — **NOT contingent upon the presence of a monopole.**

- **Based on:**
  D. Zhu, X. Chen and K. M. Wong, *Phys. Rev. D* **113**, 053004 (2026); arXiv:2605.20791 (*JHEP*, under review).

The Models: Weinberg-Salam vs. SU(2) YMH

In mostly positive convention, $(-,+,+,+)$:

- Lagrangian for the bosonic sector of the Weinberg-Salam (WS) theory is

$$\mathcal{L} = -\frac{1}{4}F^a_{\mu\nu}F^{a\mu\nu} - \frac{1}{4}f_{\mu\nu}f^{\mu\nu} - (\mathcal{D}_\mu\phi)^\dagger(\mathcal{D}^\mu\phi) - \frac{\lambda}{2}\left(\phi^\dagger\phi - \frac{\mu_H^2}{\lambda}\right)^2,$$

  where the covariant derivative of the SU(2)×U(1) group is given by

$$\mathcal{D}_\mu = \partial_\mu - \frac{i}{2}gA^a_\mu\sigma^a - \frac{i}{2}g'B_\mu. \tag{1}$$

- For the SU(2) Yang-Mills-Higgs (YMH) theory:

$$\mathcal{L} = -\frac{1}{4}F^a_{\mu\nu}F^{a\mu\nu} - \frac{1}{2}D_\mu\Phi^a D^\mu\Phi^a - \frac{\lambda}{4}\left(\Phi^a\Phi^a - \frac{\mu_H^2}{\lambda}\right)^2,$$

  where the covariant derivative of the Higgs field is

$$D_\mu\Phi^a = \partial_\mu\Phi^a + g\varepsilon^{abc}A^b_\mu\Phi^c.$$

The corresponding equations of motion are

- For the WS theory, there are three:

$$\mathcal{D}_\mu \mathcal{D}^\mu \phi = \lambda \left(\phi^\dagger \phi - \frac{\mu_H^2}{\lambda} \right) \phi,$$

$$D^\mu F^a_{\mu\nu} = \frac{ig}{2} \left[\phi^\dagger \sigma^a \left(\mathcal{D}_\nu \phi \right) - \left(\mathcal{D}_\nu \phi \right)^\dagger \sigma^a \phi \right],$$

$$\partial^\mu f_{\mu\nu} = \frac{ig'}{2} \left[\phi^\dagger \left(\mathcal{D}_\nu \phi \right) - \left(\mathcal{D}_\nu \phi \right)^\dagger \phi \right].$$

- For the YMH theory, there are only two:

$$D^\mu F^a_{\mu\nu} = g \varepsilon^{abc} \Phi^b D_\nu \Phi^c,$$

$$D^\mu D_\mu \Phi^a = \lambda \Phi^a \left(\Phi^b \Phi^b - \frac{\mu_H^2}{\lambda} \right).$$

The Axially Symmetric Magnetic Ansatz

To obtain the Cho-Maison and SU(2) MAP numerical solutions, the following ansätze are applied:

- The SU(2) gauge potential:

$$gA_i^a = -\frac{1}{r}\psi_1(r,\theta)\,\hat{\boldsymbol{n}}_\phi^a\hat{\boldsymbol{\theta}}_i + \frac{n}{r}\psi_2(r,\theta)\,\hat{\boldsymbol{n}}_\theta^a\hat{\boldsymbol{\phi}}_i + \frac{1}{r}R_1(r,\theta)\,\hat{\boldsymbol{n}}_\phi^a\hat{\boldsymbol{r}}_i - \frac{n}{r}R_2(r,\theta)\,\hat{\boldsymbol{n}}_r^a\hat{\boldsymbol{\phi}}_i,$$
$$A_0^a = \tau_1(r,\theta)\,\hat{\boldsymbol{n}}_r^a + \tau_2(r,\theta)\,\hat{\boldsymbol{n}}_\theta^a = 0.$$

- The U(1) gauge potential:

$$g'B_i = \frac{n}{r\cdot\sin\theta}B_s(r,\theta)\,\hat{\boldsymbol{\phi}}_i, \qquad B_0 = B_0(r,\theta) = 0.$$

- The Higgs field:

$$\Phi^a = \Phi_1(r,\theta)\,\hat{\boldsymbol{n}}_r^a + \Phi_2(r,\theta)\,\hat{\boldsymbol{n}}_\theta^a = \frac{H(r,\theta)}{\sqrt{2}}\hat{\boldsymbol{\Phi}}^a,$$

  where

$$\hat{\boldsymbol{\Phi}}^a = -\boldsymbol{\xi}^\dagger\sigma^a\boldsymbol{\xi} \quad \text{and} \quad \boldsymbol{\xi} = \mathrm{i}\begin{pmatrix}\sin\frac{\alpha(r,\theta)}{2}e^{-\mathrm{i}n\phi}\\ -\cos\frac{\alpha(r,\theta)}{2}\end{pmatrix}.$$

  Here, $\alpha(r,\theta)$ is the Higgs inclination angle in the SU(2) internal space, which approaches 2θ asymptotically for the MAP configurations studied in this work. Lastly, $\phi = H\boldsymbol{\xi}/\sqrt{2}$, where $H = |\Phi| = \sqrt{\Phi_1^2 + \Phi_2^2}$ is the Higgs modulus.

Detailed Numerical Methods

1. **Rescale** the Higgs field: $H = \widetilde{H} H_0$, with $H_0 = \sqrt{2}\mu_H/\sqrt{\lambda}$.

2. **Transform** the radial coordinate: $r = x/m_W$, with $m_W = gH_0/2$.
   Note: $m_W^{-1} \approx 2.5$ am — the characteristic range of weak interactions, more than 600 times smaller than a proton.

3. Only **two** dimensionless parameters survive:
   - $\tan\theta_W = g'/g \approx 0.5358$ $(\cos\theta_W = m_W/m_Z)$
   - $\beta = \sqrt{\lambda}/g = m_H/(2m_W) \approx 0.7782$

   Note: Calculated according to data published by the Particle Data Group in 2020.

4. **Compactify** the radial axis: $x_c = x/(x+1)$.

5. **Discretize** onto a 70×60 mesh: $0 \le x_c \le 1$ (70 radial), $0 \le \theta \le \pi$ (60 angular).

6. Standard practice of finite differences, a Jacobian matrix, boundary conditions, and a suitable initial guess.

Boundary Conditions

- Asymptotically, at $r = \infty$ (corresponds to $x_c = 1$):

$$\psi_A(\infty, \theta) = 2, R_A(\infty, \theta) = 0, \; B_s(\infty, \theta) = 0,$$
$$\Phi_1(\infty, \theta) = \cos\theta, \Phi_2(\infty, \theta) = \sin\theta.$$

- At the origin, when $r = 0$ (corresponds to $x_c = 0$):

$$\psi_A(0, \theta) = R_A(0, \theta) = 0, \; B_s(0, \theta) = -2,$$
$$\Phi_1(0, \theta)\sin\theta + \Phi_2(0, \theta)\cos\theta = 0,$$
$$\partial_r(\Phi_1(r, \theta)\cos\theta - \Phi_2(r, \theta)\sin\theta)|_{r=0} = 0.$$

- Along the z-axis ($\theta = 0, \pi$):

$$\partial_\theta\psi_A = R_A = \partial_\theta\Phi_1 = \Phi_2 = \partial_\theta B_s = 0.$$

Note: $A = 1, 2$ in the above expressions.

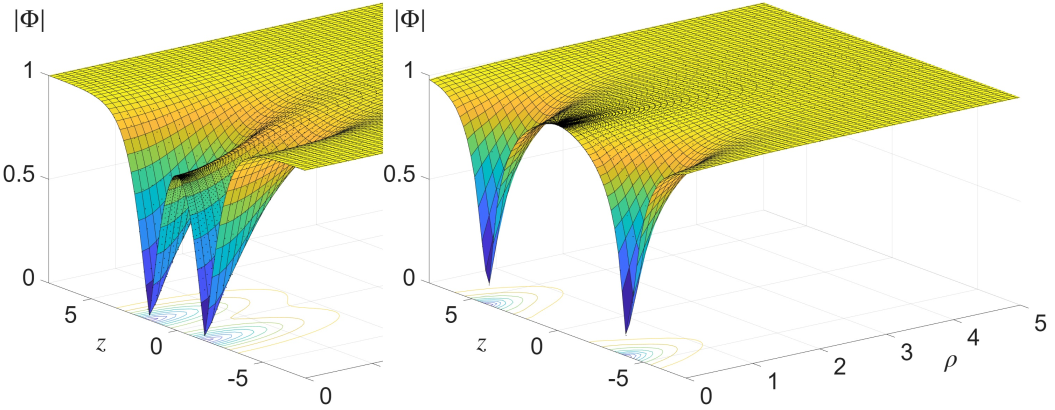

Figure 1: 3D Higgs modulus comparison between an SU(2) MAP (left) and a Cho-Maison MAP (right). In both cases, $n = 1$.

The MAP configurations are located along the z-axis with $\rho = \sqrt{x^2 + y^2}$. Note that the pole separation, d_z, for a Cho-Maison MAP is significantly wider.

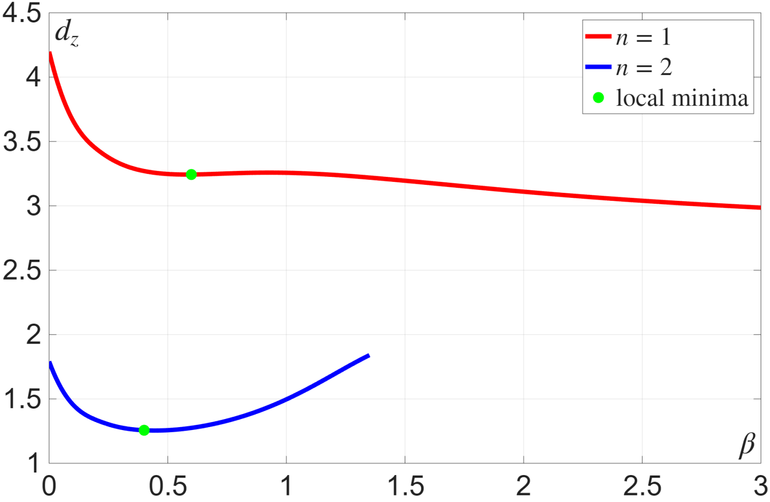

Figure 2: Pole separation d_z vs. Higgs self-coupling β for SU(2) MAP solutions with different ϕ-winding number n.

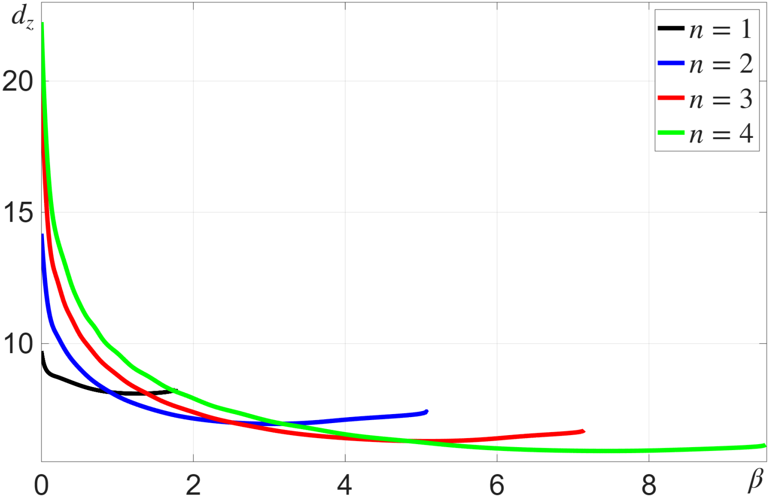

Figure 3: Pole separation d_z vs. Higgs self-coupling β for Cho-Maison MAP solutions with different ϕ-winding number n.

To study the counter-intuitive behavior of d_z in the Cho-Maison MAP, we investigated the last diagonal component of the energy-momentum tensor, T_{33}.

- In the WS theory, the energy-momentum tensor is given by

$$T_{\mu\nu} = 2\left(\mathcal{D}_\mu\phi\right)^\dagger\left(\mathcal{D}_\nu\phi\right) + F^a_{\mu\beta}F^{a\beta}_\nu + f_{\mu\beta}f^\beta_\nu + g_{\mu\nu}\mathcal{L},$$

  and therefore, the full expression for T_{33} is

$$\begin{aligned} T_{33} &= 2\left(\mathcal{D}_3\phi\right)^\dagger\left(\mathcal{D}_3\phi\right) - \left(\mathcal{D}_i\phi\right)^\dagger\left(\mathcal{D}^i\phi\right) - \frac{\lambda}{2}\left(\phi^\dagger\phi - \frac{\mu_H^2}{\lambda}\right)^2 + \left(F^a_{3i}F^{ai}_3 - \frac{1}{4}F^a_{ij}F^{aij}\right) + \left(f_{3i}f^i_3 - \frac{1}{4}f_{ij}f^{ij}\right) \\ &= T^{\mathrm{Higgs}}_{33} + T^{\mathrm{SU(2)}}_{33} + T^{\mathrm{U(1)}}_{33}. \end{aligned} \tag{2}$$

- Similarly, in the YMH theory,

$$T_{\mu\nu} = D_\mu\Phi^a D_\nu\Phi^a + F^a_{\mu\beta}F^{a\beta}_\nu + g_{\mu\nu}\mathcal{L}$$

  and hence, the last diagonal component is

$$T_{33} = D_3\Phi^a D_3\Phi^a - \frac{1}{2}D_i\Phi^a D^i\Phi^a - \frac{\lambda}{4}\left(\Phi^a\Phi^a - \frac{\mu_H^2}{\lambda}\right)^2 + \left(F^a_{3i}F^{ai}_3 - \frac{1}{4}F^a_{ij}F^{aij}\right) = T^{\mathrm{Higgs}}_{33} + T^{\mathrm{SU(2)}}_{33}.$$

In the WS theory, the physical and fundamental fields are related through:

$$\begin{pmatrix} A_i^{\mathrm{em}} \\ Z_i \end{pmatrix} = \begin{pmatrix} \cos\theta_W & \sin\theta_W \\ -\sin\theta_W & \cos\theta_W \end{pmatrix} \begin{pmatrix} B_i \\ A_i'^3 \end{pmatrix},$$

with inverse relations:

$$B_i = \cos\theta_W A_i^{\mathrm{em}} - \sin\theta_W Z_i,$$
$$A_i'^3 = \sin\theta_W A_i^{\mathrm{em}} + \cos\theta_W Z_i.$$

From the covariant derivative structure shown in Eq. (1), the T_{33}^{Higgs} component in Eq. (2) contains:

1. Direct Higgs contributions: $(\partial_3\phi)^2$
2. Gauge-Higgs couplings: $(A_i^a\sigma^a\phi)^2$, ...
3. Cross terms: $(A_i^a\sigma^a\phi)^\dagger\,(B^i\phi)$, ...

This shows that T_{33}^{Higgs} incorporates both pure Higgs contribution and interactions between Higgs, Z-boson, and electromagnetic fields.

Results & Discussion — T_{33}^{Higgs}

SU(2) MAP

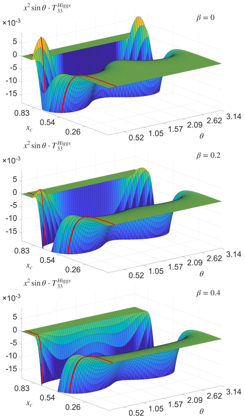

Figure 4: Evolution of the asymptotic repulsive contribution (large x_c) in YMH $x^2 \sin\theta \cdot T_{33}^{\mathrm{Higgs}}$ with the vertical axis fixed at $[-0.018, 0.009]$ for $\beta =$ (a) 0, (b) 0.2, (c) 0.4.

Cho-Maison MAP

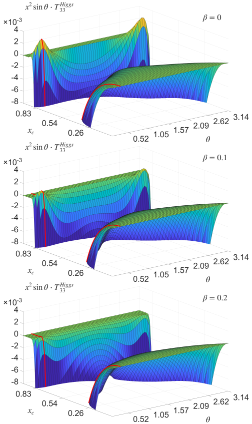

Figure 5: Evolution of the asymptotic repulsive contribution (large x_c) in WS $x^2 \sin\theta \cdot T_{33}^{\mathrm{Higgs}}$ with the vertical axis fixed at $[-0.008, 0.004]$ for $\beta =$ (a) 0, (b) 0.1, (c) 0.2 ($\tan\theta_W = 1$).

Results & Discussion — YMH T_{33}: β Dependence

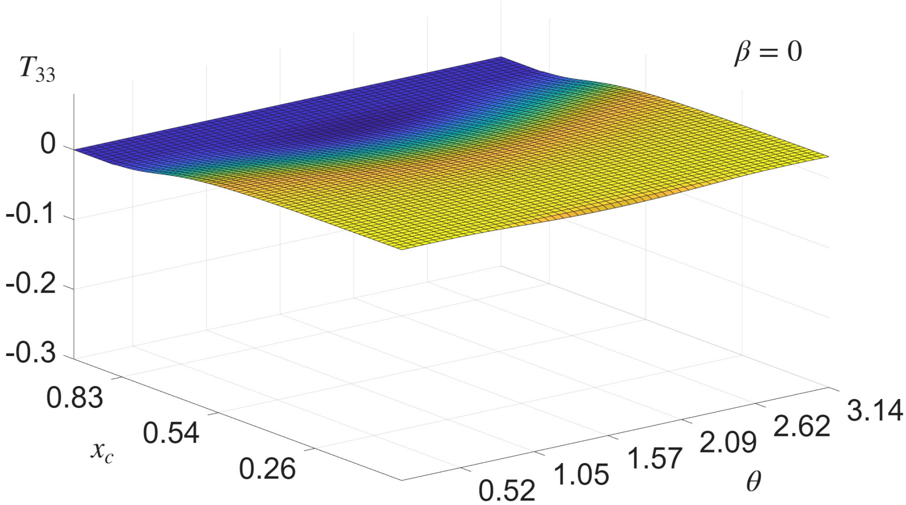

The evolution of $T_{33} = T_{33}^{\mathrm{Higgs}} + T_{33}^{\mathrm{SU(2)}}$ distribution for an SU(2) MAP, $\beta = 0$.

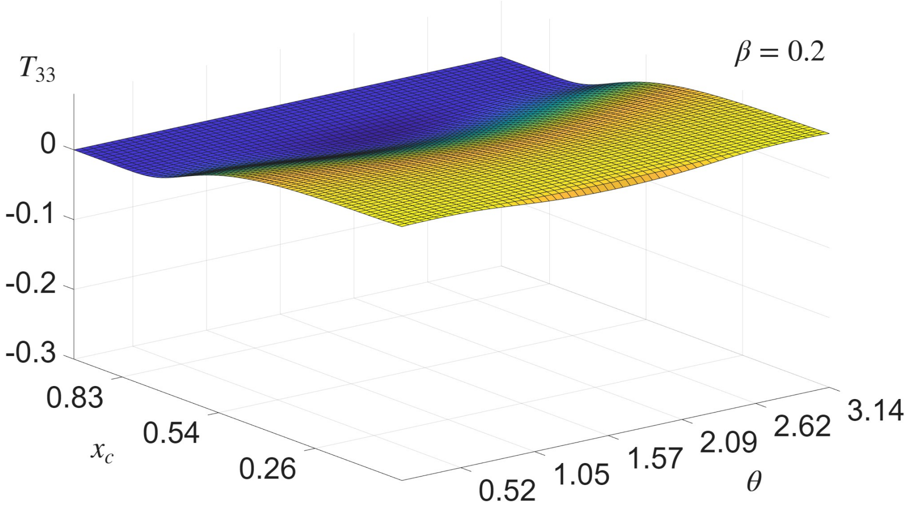

The evolution of $T_{33} = T_{33}^{\mathrm{Higgs}} + T_{33}^{\mathrm{SU(2)}}$ distribution for an SU(2) MAP, $\beta = 0.2$.

Results & Discussion — YMH T_{33}: β Dependence

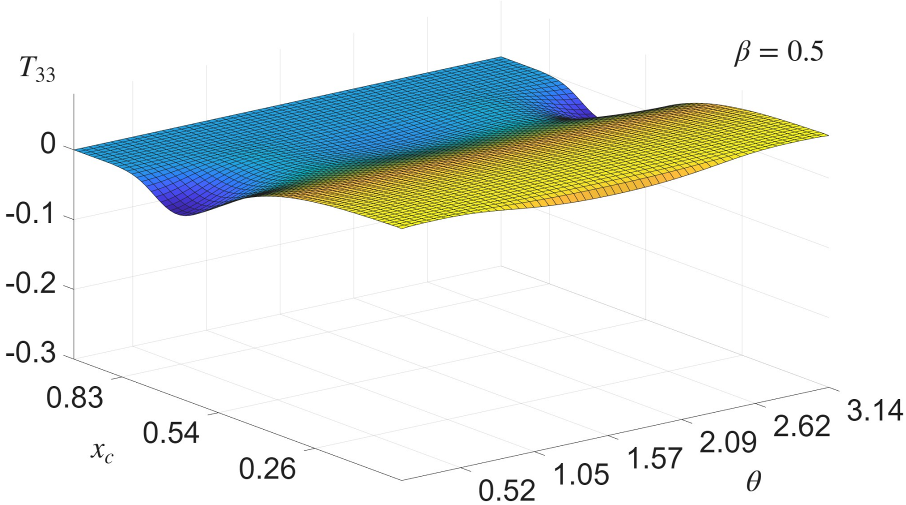

The evolution of $T_{33} = T_{33}^{\mathrm{Higgs}} + T_{33}^{\mathrm{SU(2)}}$ distribution for an SU(2) MAP, $\beta = 0.5$.

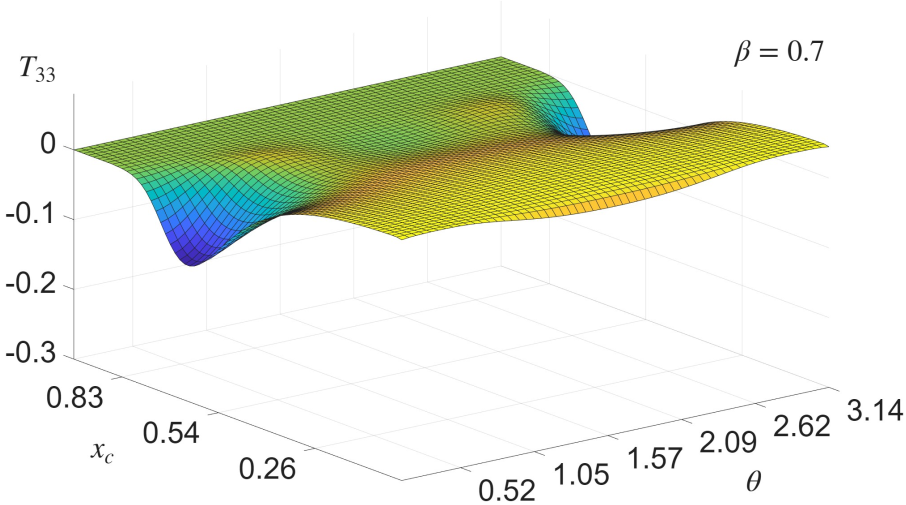

The evolution of $T_{33} = T_{33}^{\mathrm{Higgs}} + T_{33}^{\mathrm{SU(2)}}$ distribution for an SU(2) MAP, $\beta = 0.7$.

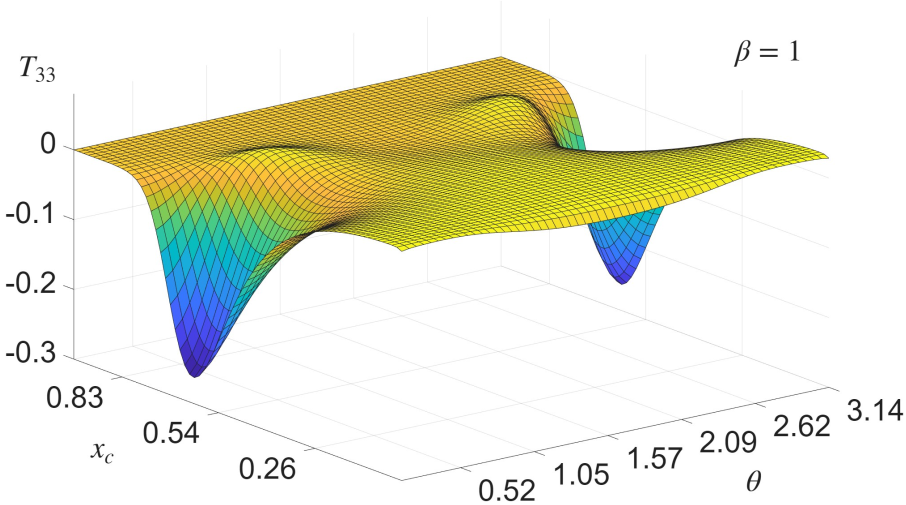

The evolution of $T_{33} = T_{33}^{\mathrm{Higgs}} + T_{33}^{\mathrm{SU(2)}}$ distribution for an SU(2) MAP, $\beta = 1$.

Results & Discussion — YMH $\int T_{33}\, d^3x$

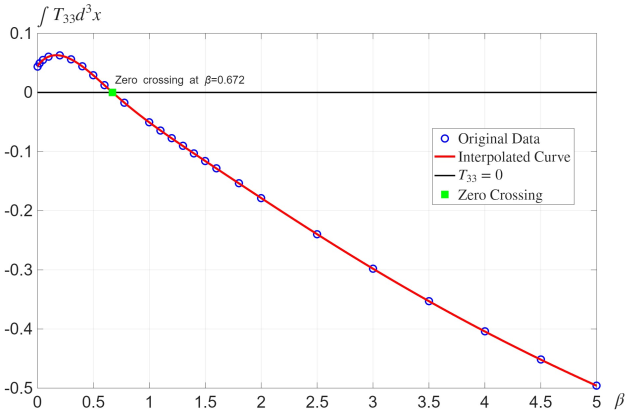

Figure 6: Plot of the integrated T_{33} versus Higgs self-coupling β for SU(2) MAP solutions with $n = 1$.

Sign change: the value of $\int T_{33}\, d^3x$ turns from positive (repulsive) to negative (attractive) as β increases — the Higgs-mediated repulsion is **regulated by the Higgs mass**.

Results & Discussion — WS $T_{33}^{\mathrm{SU}(2)}$

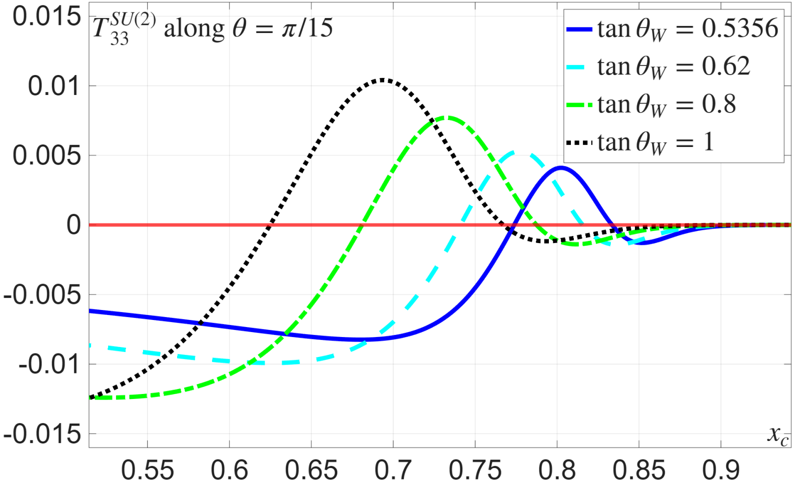

Figure 7: Cross-sections of $T_{33}^{\mathrm{SU}(2)}$ along $\theta = \pi/15$ for Cho-Maison MAP solutions with $\beta = 0.7782$ and varying $\tan\theta_W$. Repulsive interactions are localized near the pole positions, producing cores of radius $R_c \approx 0.8\, m_W^{-1}$.

Results & Discussion — Neutral Charge Density, $\mathcal{N}$

For the Cho-Maison MAP configuration, the neutral charge density is calculated as follows

$$\mathcal{N} = \partial^i \mathcal{B}_i^{\text{neutral}} = \partial^i \left(-\frac{1}{2} \varepsilon_{ijk} \mathcal{Z}^{jk} \right)$$
$$= \partial^i \left[-\frac{1}{2} \varepsilon_{ijk} \left(\partial^j Z^k - \partial^k Z^j \right) \right]$$

where $\mathcal{B}_i^{\text{neutral}}$, $\mathcal{Z}^{jk}$, and Z^j are the Z-boson neutral field, strength tensor, and potential, respectively.

Figure on the right provides direct evidence for Z-boson exchange between monopole and antimonopole in the Cho-Maison MAP configuration.

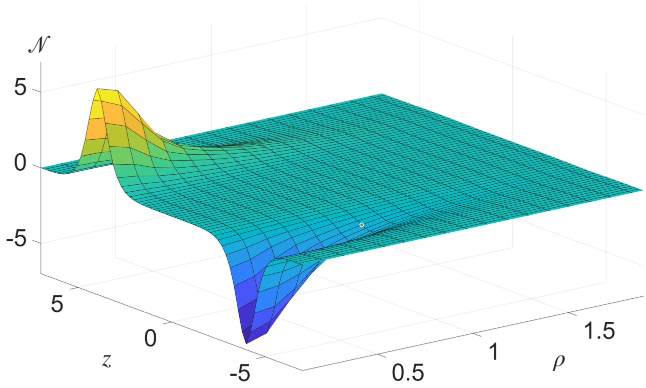

Figure 8: 3D neutral charge density, $\mathcal{N}$, for Cho-Maison MAP solution with $\beta = 0.7782$, $\tan\theta_W = 0.5358$, and $n = 1$.

Results & Discussion — Electroweak Vortex Rings

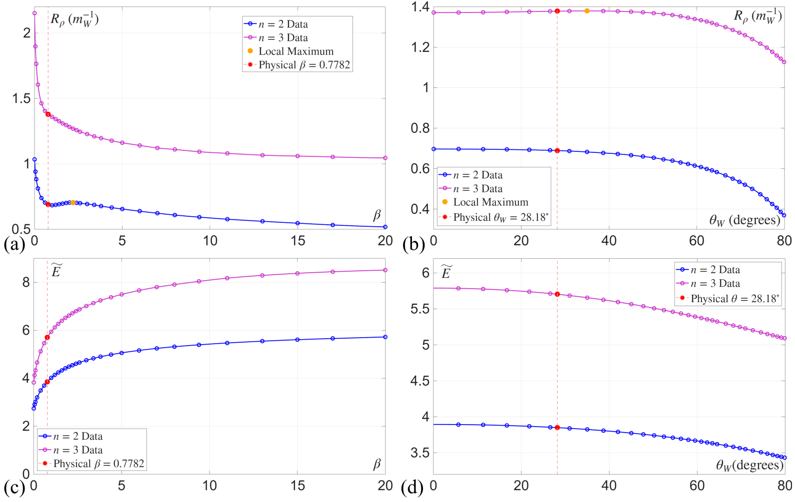

Figure 9: Dependence of vortex ring properties on model parameters. For a detailed explanation, please refer to arXiv:2605.20791.

Conclusion

In this work, through comparisons with the SU(2) MAPs, we identified two distinct repulsive mechanisms in the Cho-Maison MAP configurations:

1. **Higgs-mediated repulsion** shows a non-monotonic dependence on both n and β: the n-dependence confirms its *topological origin*, while the β-dependence reveals structure beyond simple Yukawa suppression. Its magnitude is comparable to the Coulomb-like magnetic attraction.
2. ***Z*-boson-mediated repulsion** originates purely from weak interactions, producing localized cores of radius $R_c \approx 0.8\, m_W^{-1}$ that align with the characteristic weak interaction scale ($m_Z^{-1} = m_W^{-1} \cos\theta_W \approx 0.88\, m_W^{-1}$). This confirms Z-boson exchange as a weak interaction mediator between topological defects.

These two mechanisms collectively counterbalance the magnetic attraction between the Cho-Maison monopole and antimonopole, holding them at a finite pole separation. Recently, we found that the same interpretation extends naturally to electroweak vortex rings (arXiv:2605.20791) — there too, the size of those configurations is governed by these repulsive interactions.

Thank you for your attention!